Comparison of Path Tracking and Torque-Vectoring Controllers for Autonomous Electric Vehicles

Christoforos Chatzikomis, Aldo Sorniotti, *Member, IEEE*, Patrick Gruber, Mattia Zanchetta, Dan Willans, and Bryn Balcombe

***Abstract*—Steering control for path tracking in autonomous vehicles is well documented in the literature. Also, continuous direct yaw moment control, i.e., torque-vectoring, applied to human-driven electric vehicles with multiple motors is extensively researched. However, the combination of both controllers is not yet well understood. This paper analyzes the benefits of torque-vectoring in an autonomous electric vehicle, either by integrating the torque-vectoring system into the path tracking controller, or through its separate implementation alongside the steering controller for path tracking. A selection of path tracking controllers is compared in obstacle avoidance tests simulated with an experimentally validated vehicle dynamics model. A genetic optimization is used to select the controller parameters. Simulation results confirm that torque-vectoring is beneficial to autonomous vehicle response. The integrated controllers achieve the best performance if they are tuned for the specific tire-road friction condition. However, they can also cause unstable behavior when they operate under lower friction conditions without any re-tuning. On the other hand, separate torque-vectoring implementations provide a consistently stable cornering response for a wide range of friction conditions. Controllers with preview formulations, or based on appropriate reference paths with respect to the middle line of the available lane, are beneficial to the path tracking performance.**

***Index Terms*—Autonomous vehicle, electric vehicle, path tracking control, torque-vectoring control, optimization, vehicle dynamics.**

I. Introduction

AUTONOMOUS vehicles require path tracking controllers (PTCs) that ensure safe behavior even in extreme maneuvers. Most of the path tracking (PT) studies (see the survey in [1]) focus on steering actuation. A large body of literature on steering control for PT was initially developed with the purpose of driver modeling [2]–[7]. In fact, the human driver can be seen as an advanced adaptive PTC actuating the steering wheel. Hence, driver models can perform as automated PTCs as well, provided that human physiology limitations are not considered in their formulations. In recent years the research focus has shifted from driver modeling to autonomous driving applications [8]–[14]. In this respect, [15] compares the performance of multiple steering based PTCs for autonomous vehicles.

Another topic extensively discussed in the literature is torque-vectoring (TV), i.e., the control of the traction and braking torque of each wheel to generate a direct yaw moment. TV controllers (TVCs) are easily implementable in electric vehicles (EVs) with individual wheel motors, since these solutions allow precise wheel torque controllability, usually with higher bandwidth than the conventional friction brakes and internal combustion engine drivetrains. In human driven EVs, TVCs can enhance the cornering response, e.g., by shaping the understeer characteristic, increasing agility and ensuring stability in extreme transients [16]–[23]. TVCs are usually implemented as yaw rate feedforward / feedback controllers, with the option of sideslip contributions.

In autonomous EVs the TVC can be an independent controller receiving the automated steering angle as an input from the PTC, and thus generating a reference yaw rate that has to be tracked by the TVC itself [24]. Alternatively, steering actuation and TV can be merged to become the outputs of an integrated PTC, without the need for a reference yaw rate to be tracked by the TVC. In this respect, [25]–[31] propose PTCs with integrated steering and direct yaw moment control. [32] is a comparative study between model predictive control (MPC) and a linear quadratic regulator (LQR) for integrated PTC, tuned through a trial-and-error process. However, it is yet unknown if the integrated PTCs present benefits compared to the multi-layer control structures consisting of independent steering controllers for PT (top layer) and TVCs for yaw rate and sideslip tracking (bottom layer).

This study addresses this knowledge gap by assessing the two architectural control system designs during obstacle avoidance maneuvers simulated with an experimentally validated vehicle simulation model. The points of novelty are:

- The integration of TV with multiple steering based PTCs from the literature. Both single-point PTCs without preview and multiple-point preview PTCs are used.
- The stochastic optimization of the PTC parameters to achieve a fair comparison among the control structures.
- The objective comparison of the performance of the separate and integrated steering and yaw moment controllers.

Manuscript received October 19, 2017; revised March 21, 2018; accepted May 13, 2018. Date of publication October 8, 2018; date of current version November 21, 2018. *(Corresponding author: Aldo Sorniotti.)*

A. Sorniotti, P. Gruber, and M. Zanchetta are with the University of Surrey, Guildford GU2 7XH, U.K. (e-mail: a.sorniotti@surrey.ac.uk; p.gruber@surrey.ac.uk; m.zanchetta@surrey.ac.uk).

C. Chatzikomis, D. Willans, and B. Balcombe are with Roborace, Oxford OX16 4XD, U.K. (e-mail: christoforos@roborace.com; willans@roborace.com; bryn@roborace.com).

Color versions of one or more of the figures in this paper are available online at http://ieeexplore.ieee.org.

Digital Object Identifier 10.1109/TIV.2018.2874529

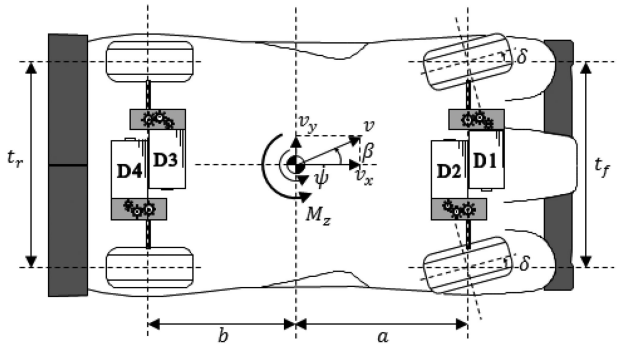

Fig. 1. Layout of the case study autonomous EV.

TABLE I
MAIN EV PARAMETERS

Parameter	Value / description
Vehicle mass	1250 kg
Front semi-wheelbase	1.6 m
Rear semi-wheelbase	1.3 m
Front track width	1.55 m
Rear track width	1.55 m
Front tires	295/30 ZR18 Michelin Pilot Sport Cup 2
Rear tires	345/30 ZR20 Michelin Pilot Sport Cup 2
Powertrains	4 on-board 135 kW electric motors
Transmission gear ratio	6.25:1

II. THE CASE STUDY AUTONOMOUS ELECTRIC VEHICLE

A. EV Hardware

The case study vehicle is an autonomous EV prototype, developed for a new racing competition. Fig. 1 and Table I present the EV layout, and define the main characteristics and variables. The powertrain architecture consists of four on-board electric drivetrains (D1 to D4 in Fig. 1), coupled with single-speed gearboxes connected to the wheels through half-shafts and constant-velocity joints. Front and rear wings generate significant aerodynamic downforce, which increases the maximum longitudinal and lateral accelerations. Also, the downforce changes the steady-state cornering response, i.e., the level of under/oversteer, as a function of speed.

The EV is equipped with a comprehensive set of sensors that enable PT control. In addition, the EV includes an inertia measurement unit that measures the linear accelerations and angular speeds in all directions, and an optical velocity sensor that detects the longitudinal and lateral speeds.

B. Control System Hierarchy

The control structure of the autonomous EV, shown in Fig. 2, includes:

- The sensor fusion system collecting the signals from the sensors located on the EV, and estimating/calculating the inputs required by the different control blocks.
- The path generator defining the coordinates of the reference path, X_{ref} and Y_{ref}, and the reference speed profile, $v_{x,ref}$.
- The PTC, which calculates the control actions for tracking the reference path. The controller outputs the total wheel torque demand, $T_{w,tot}$, steering angle, δ, and, only in case of an integrated control structure, the reference yaw moment, $M_{z,ref}$.
- The TVC, present only in case of a multi-layer control structure, and indicated with dashed lines in Fig. 2. The TVC consists of a reference yaw rate ($\dot{\psi}^{TVC}_{ref}$) generator, and a reference yaw moment ($M_{z,ref}$) generator.
- The wheel torque control allocator, which generates the individual wheel torques $T_{w,i}$, to achieve $T_{w,tot}$ and $M_{z,ref}$ [24].

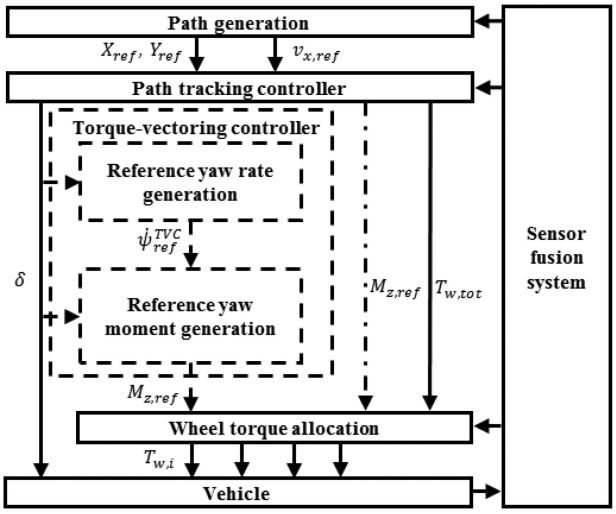

Fig. 2. Simplified schematic of the autonomous EV control structure.

III. PATH TRACKING CONTROLLERS

The PTCs output the longitudinal and lateral control actions to track the reference path. Since this study focuses on obstacle avoidance maneuvers [33], which are performed with $T_{w,tot} = 0$, only the lateral control formulations are presented.

A. Reference Path and Vehicle Coordinates

The reference path can be dynamically planned by the path generator, accounting for the EV navigation objectives, road and traffic constraints, and potential obstacles. This study uses a static reference path, as the focus is on the PT layer.

The path tracking problem can be described as in Fig. 3. X_{ref} and Y_{ref} are the reference path coordinates. They are expressed in the global coordinate system, and are sufficient to uniquely define the reference path. In the remainder the capital letters X and Y will be used to express coordinates in the global reference system, while x and y will be adopted for coordinates in the vehicle reference system. The reference heading (yaw) angle, ψ_{ref}, and the reference curvature, κ_{ref}, are derived from the reference coordinates and used by the PTCs.

Since the EV deviates from the reference path, the actual distance traveled by the EV, s, is not equal to the length of the reference path. By assuming small sideslip angles, the distance travelled along the reference path during the maneuver is given by [7], eqn. (1) shown at the bottom of the next page:

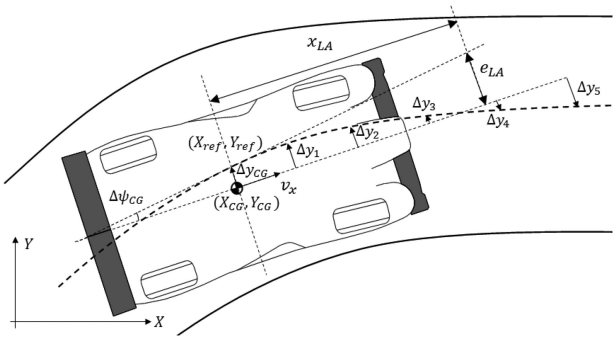

Fig. 3. EV reference path coordinates and relative position and heading errors.

where v_x and v_y are the longitudinal and lateral EV speeds, and X_{CG} and Y_{CG} are the coordinates of the vehicle center of gravity (CG). The lateral position error, Δy_{CG}, and heading angle error, $\Delta\psi_{CG}$, of the EV CG in relation to the reference path are defined as in Fig. 3:

$$\begin{aligned}\Delta y_{CG} &= (Y_{CG} - Y_{ref})\cos\psi_{ref} - (X_{CG} - X_{ref})\sin\psi_{ref}\\ \Delta\psi_{CG} &= \psi - \psi_{ref}\end{aligned} \tag{2}$$

where ψ is the EV heading angle.

B. $FF\text{-}FB_\delta$: Feedforward-Feedback Steering Controller

The first PTC of this study is the feedforward-feedback controller, $FF\text{-}FB_\delta$, recently presented in [34], which has been experimentally demonstrated at the limit of handling. The steering angle control law consists of feedforward and feedback contributions:

$$\delta = \delta_{FF} + \delta_{FB} \tag{3}$$

The feedforward term, δ_{FF}, is based on the steady-state cornering response of the single-track vehicle model:

$$\delta_{FF} = l\kappa_{ref} - \left(\alpha_F^{FF} - \alpha_R^{FF}\right) \tag{4}$$

where l is the wheelbase. The term $l\kappa_{ref}$ is the kinematic steering angle corresponding to the reference path curvature. α_F^{FF} and α_R^{FF} are the lumped slip angles of the front and rear tires. α_F^{FF} and α_R^{FF} are calculated from an inverse tire model, taking into account the vertical load transfers, so that they generate the respective feedforward lateral tire forces on the front and rear axles, $F_{y,F}^{FF}$ and $F_{y,R}^{FF}$. These are determined under the assumption that the vehicle achieves the reference lateral acceleration, ${v_x}^2\kappa_{ref}$, calculated for steady-state cornering. Based on the lateral force and yaw moment balance equations in steady-state conditions, $F_{y,F}^{FF}$ and $F_{y,R}^{FF}$ are:

$$\begin{cases} F_{y,F}^{FF} = \dfrac{mb}{l}\,{v_x}^2\kappa_{ref} - \dfrac{M_{z,ref}}{l} \\ F_{y,R}^{FF} = \dfrac{ma}{l}\,{v_x}^2\kappa_{ref} + \dfrac{M_{z,ref}}{l} \end{cases} \tag{5}$$

where m is the vehicle mass, and a and b are the front and rear semi-wheelbases.

The feedback term, δ_{FB}, is designed to control the corrected look-ahead error, $e_{LA,corr}$, and is defined as:

$$\begin{aligned}\delta_{FB} &= -K_{FF\text{-}FB_\delta}\, e_{LA,corr}\\ &= -K_{FF\text{-}FB_\delta}\,\left[\Delta y_{CG} + x_{LA}\left(\Delta\psi_{CG} + \beta_{ss}\right)\right]\end{aligned} \tag{6}$$

$$\beta_{ss} = \alpha_R^{FF} + b\kappa_{ref} \tag{7}$$

where $K_{FF\text{-}FB_\delta}$ is the proportional (P) gain. The term $e_{LA} = \Delta y_{CG} + x_{LA}\Delta\psi_{CG}$ is the look-ahead error, i.e., the tracking error projected at a distance x_{LA} in front of the vehicle, as shown in Fig. 3. For the lateral deviation to be zero, the vehicle sideslip angle β is incorporated in the feedback law, which is then based on $e_{LA,corr}$. To avoid relying on the real-time measurement or estimation of β, as suggested in [34] eq. (6) uses β_{ss}, which is the steady-state value of β corresponding to the reference curvature, according to eq. (7).

C. LQR_{δ,M_z}: Linear Quadratic Regulator Without Preview (Integrated Controller)

The second controller is based on the LQR formulation for steering control in [15], which is extended to include the reference yaw moment.

The state-space formulation of the single-track vehicle model for path tracking control is:

$$\begin{aligned}\begin{bmatrix}\Delta\dot{y}_{CG}\\ \Delta\ddot{y}_{CG}\\ \Delta\dot{\psi}_{CG}\\ \Delta\ddot{\psi}_{CG}\end{bmatrix} &= \begin{bmatrix}0 & 1 & 0 & 0\\ 0 & -\frac{C_f+C_r}{m v_x} & \frac{C_f+C_r}{m} & \frac{bC_r-aC_f}{m v_x}\\ 0 & 0 & 0 & 1\\ 0 & \frac{bC_r-aC_f}{I_z v_x} & \frac{aC_f-bC_r}{I_z} & -\frac{a^2C_f+b^2C_r}{I_z v_x}\end{bmatrix}\\ &\times\begin{bmatrix}\Delta y_{CG}\\ \Delta\dot{y}_{CG}\\ \Delta\psi_{CG}\\ \Delta\dot{\psi}_{CG}\end{bmatrix} + \begin{bmatrix}0 & 0\\ \frac{C_f}{m} & 0\\ 0 & 0\\ \frac{aC_f}{I_z} & \frac{1}{I_z}\end{bmatrix}\begin{bmatrix}\delta\\ M_z\end{bmatrix}\\ &+\begin{bmatrix}0\\ \frac{bC_r-aC_f}{m v_x} - v_x\\ 0\\ -\frac{a^2C_f+b^2C_r}{I_z v_x}\end{bmatrix}\dot{\psi}_{ref} + \begin{bmatrix}0\\ 0\\ 0\\ -1\end{bmatrix}\ddot{\psi}_{ref}\end{aligned} \tag{8}$$

where I_z is the yaw mass moment of inertia. C_f and C_r are the cornering stiffness values of the front and rear axles. In this study, these are selected at a specific percentage, $p_{a_{y,max}}$, of the maximum a_y achieved in steady-state conditions, according to the approach in [35]. In eq. (8) the state variables of the

$$s = \int \frac{v_x\cos\left(\Delta\psi_{CG}\right) - v_y\sin\left(\Delta\psi_{CG}\right)}{1 - \kappa_{ref}\left[\left(Y_{CG} - Y_{ref}\right)\cos\psi_{ref} - \left(X_{CG} - X_{ref}\right)\sin\psi_{ref}\right]}\,dt \tag{1}$$

single-track vehicle model, i.e., v_y and $\dot{\psi}$, are converted into the error state variables with respect to the reference path:

$$\begin{aligned} v_y &= \Delta\dot{y}_{CG} - v_x\,\Delta\psi_{CG} \\ \dot{\psi} &= \Delta\dot{\psi}_{CG} + \dot{\psi}_{ref} \end{aligned} \tag{9}$$

Eq. (8) can be re-written in the following matrix form:

$$\dot{\boldsymbol{X}} = \boldsymbol{A}\boldsymbol{X} + \boldsymbol{B}_1\boldsymbol{U} + \boldsymbol{B}_2\dot{\psi}_{ref} + \boldsymbol{B}_3\ddot{\psi}_{ref}$$

$$\text{where } \boldsymbol{X} = \begin{bmatrix} \Delta y_{CG} \\ \Delta\dot{y}_{CG} \\ \Delta\psi_{CG} \\ \Delta\dot{\psi}_{CG} \end{bmatrix} \text{ and } \boldsymbol{U} = \begin{bmatrix} \delta \\ M_z \end{bmatrix} \tag{10}$$

The terms associated with the reference path yaw rate and acceleration, $\boldsymbol{B}_2\dot{\psi}_{ref}$ and $\boldsymbol{B}_3\ddot{\psi}_{ref}$, are external disturbances. The state-space formulation is discretized as:

$$\boldsymbol{X}\,(k+1) = \boldsymbol{A_k}\,\boldsymbol{X}\,(k) + \boldsymbol{B}_{1,\boldsymbol{k}}\boldsymbol{U}\,(k) \tag{11}$$

The feedback control gains minimize the cost function $J_{LQR_{\delta,M_z}}$:

$$J_{LQR_{\delta,M_z}} = \sum_{k=1}^{\infty} \boldsymbol{X}(k)^T\boldsymbol{Q}\boldsymbol{X}\,(k) + \boldsymbol{U}(k)^T\boldsymbol{R}\boldsymbol{U}\,(k)$$

$$\boldsymbol{Q} = \begin{bmatrix} q_{\Delta y_{CG}} & 0 & 0 & 0 \\ 0 & 0 & 0 & 0 \\ 0 & 0 & q_{\Delta\psi_{CG}} & 0 \\ 0 & 0 & 0 & 0 \end{bmatrix},\ \boldsymbol{R} = \begin{bmatrix} r_\delta & 0 \\ 0 & r_{M_z} \end{bmatrix} \tag{12}$$

The weighting factors $q_{\Delta y_{CG}}$ and $q_{\Delta\psi_{CG}}$ define the relative importance of the lateral displacement and heading angle errors, while r_δ and r_{M_z} define the relative significance of the steering angle and yaw moment control efforts. The feedback gains, $\boldsymbol{K}$, calculated with the Riccati equation [36], are scheduled with vehicle speed, v_x, which is a parameter in eq. (11). The feedback control law is expressed as a function of the lateral position and heading angle errors, and their time derivatives:

$$\begin{bmatrix} \delta_{FB} \\ M_{z,FB} \end{bmatrix} = \boldsymbol{K}\,(v_x) \begin{bmatrix} \Delta y_{CG} \\ \Delta\dot{y}_{CG} \\ \Delta\psi_{CG} \\ \Delta\dot{\psi}_{CG} \end{bmatrix}$$

$$\boldsymbol{K}\,(v_x) = \begin{bmatrix} k_{\delta,\Delta y_{CG}} & k_{\delta,\Delta\dot{y}_{CG}} & k_{\delta,\Delta\psi_{CG}} & k_{\delta,\Delta\dot{\psi}_{CG}} \\ k_{M_z,\Delta y_{CG}} & k_{M_z,\Delta\dot{y}_{CG}} & k_{M_z,\Delta\psi_{CG}} & k_{M_z,\Delta\dot{\psi}_{CG}} \end{bmatrix} \tag{13}$$

The LQR_{δ,M_z} can be combined with a feedforward contribution in terms of steering angle and yaw moment, thus giving origin to the $LQR_{\delta,M_z,FF}$. The same formulation as in eq. (4) is used for the feedforward steering contribution, δ_{FF}. The reference yaw acceleration, $\ddot{\psi}_{ref}$, corresponding to the time derivative of the curvature of the reference path, is adopted for the feedforward yaw moment contribution, $M_{z,FF}$:

$$\begin{aligned} M_{z,FF} &= c_{M_{z,FF}}\ \ddot{\psi}_{ref} I_z \\ \ddot{\psi}_{ref} &= v_x\,\dot{\kappa}_{ref} \end{aligned} \tag{14}$$

As $\ddot{\psi}_{ref}$ has to be generated by the total yaw moment, caused by both the longitudinal and lateral tire forces, the scaling factor $0 \le c_{M_{z,FF}} \le 1$ accounts for the fact that $M_{z,FF}$ is the feedforward yaw moment generated only by the longitudinal tire forces.

D. P-LQR$_{\delta,M_z}$: Linear Quadratic Regulator With Preview (Integrated Controller)

The third controller includes a preview model according to the formulation in [37], which is limited to the case of steering control. In this study the algorithm is extended to include the yaw moment contribution. Under the hypothesis of small heading angles, the single-track vehicle model equations are reformulated in the global coordinate system as:

$$\begin{bmatrix} \dot{Y}_{CG} \\ \ddot{Y}_{CG} \\ \dot{\psi} \\ \ddot{\psi} \end{bmatrix} = \begin{bmatrix} 0 & 1 & 0 & 0 \\ 0 & -\frac{C_f+C_r}{m\,v_x} & \frac{C_f+C_r}{m} & \frac{bC_r-aC_f}{m\,v_x} \\ 0 & 0 & 0 & 1 \\ 0 & \frac{bC_r-aC_f}{I_z\,v_x} & \frac{aC_f-bC_r}{I_z} & -\frac{a^2C_f+b^2C_r}{I_z\,v_x} \end{bmatrix} \times \begin{bmatrix} Y_{CG} \\ \dot{Y}_{CG} \\ \psi \\ \dot{\psi} \end{bmatrix} + \begin{bmatrix} 0 & 0 \\ \frac{C_f}{m} & 0 \\ 0 & 0 \\ \frac{aC_f}{I_z} & \frac{1}{I_z} \end{bmatrix} \begin{bmatrix} \delta \\ M_z \end{bmatrix} \tag{15}$$

$$\dot{\boldsymbol{X}}_{\boldsymbol{v}} = \boldsymbol{A_v}\,\boldsymbol{X_v} + \boldsymbol{B_v}\boldsymbol{U}$$

$$\boldsymbol{X_v} = \begin{bmatrix} Y_{CG} \\ \dot{Y}_{CG} \\ \psi \\ \dot{\psi} \end{bmatrix},\ \boldsymbol{U} = \begin{bmatrix} \delta \\ M_z \end{bmatrix} \tag{16}$$

and then they can be discretized as:

$$\boldsymbol{X_v}\,(k+1) = \boldsymbol{A_{v,k}}\,\boldsymbol{X_v}\,(k) + \boldsymbol{B_{v,k}}\boldsymbol{U}\,(k) \tag{17}$$

The road preview profile is defined as a shift register, where $\boldsymbol{y_r}(k)$ is the vector of lateral deviations from the reference path along a preview axis in front of the vehicle, and Δy_{n_p} ($= \Delta y_5$ in Fig. 3) is the final input to the road system, i.e., the new lateral deviation value.

$$\boldsymbol{y_r}\,(k+1) = \boldsymbol{A_{r,k}}\,\boldsymbol{y_r}\,(k) + \boldsymbol{B_{r,k}}\Delta y_{n_p}$$

$$\boldsymbol{A_{r,k}} = \begin{bmatrix} 0 & 1 & 0 & 0 & \cdots & 0 \\ 0 & 0 & 1 & 0 & \cdots & 0 \\ \vdots & \vdots & \vdots & \ddots & \ddots & \vdots \\ \vdots & \vdots & \vdots & \ddots & \ddots & 0 \\ 0 & 0 & 0 & \cdots & \cdots & 1 \\ 0 & 0 & 0 & \cdots & \cdots & 0 \end{bmatrix}, \boldsymbol{B_{r,k}} = \begin{bmatrix} 0 \\ 0 \\ 0 \\ \vdots \\ 1 \end{bmatrix} \quad (18)$$

Eq. (17) and eq. (18) are combined into the state-space formulation of the preview LQR problem:

$$\begin{bmatrix} \boldsymbol{X_v}(k+1) \\ \boldsymbol{y_r}(k+1) \end{bmatrix} = \begin{bmatrix} \boldsymbol{A_{v,k}} & 0 \\ 0 & \boldsymbol{A_{r,k}} \end{bmatrix} \begin{bmatrix} \boldsymbol{X_v}(k) \\ \boldsymbol{y_r}(k) \end{bmatrix} + \begin{bmatrix} \boldsymbol{B_{v,k}} \\ 0 \end{bmatrix} \boldsymbol{U}(k) + \begin{bmatrix} 0 \\ \boldsymbol{B_{r,k}} \end{bmatrix} \Delta y_{n_p} \quad (19)$$

The state vector is defined as $\boldsymbol{Z} = [\boldsymbol{X_v}\ \boldsymbol{y_r}]^T$, and the term $[0\ \ \boldsymbol{B_{r,k}}]^T \Delta y_{n_p}$ is considered an external disturbance, such that the equations are expressed in the standard LQR form.

The LQR cost function is:

$$J_{P\text{-}LQR_{\delta,M_z}} = \sum_{k=1}^{\infty} \boldsymbol{Z}(k)^T \boldsymbol{Q} \boldsymbol{Z}(k) + \boldsymbol{U}(k)^T \boldsymbol{R} \boldsymbol{U}(k)$$

$$\text{where } \boldsymbol{R} = \begin{bmatrix} r_\delta & 0 \\ 0 & r_{M_z} \end{bmatrix}, \boldsymbol{Q} = \boldsymbol{C}^T \begin{bmatrix} q_{\Delta y_{CG}} & 0 \\ 0 & q_{\Delta \psi_{CG}} \end{bmatrix} \boldsymbol{C}$$

$$\text{and } \boldsymbol{C} = \begin{bmatrix} 1 & 0 & 0 & 0 & -1 & 0 & 0 & \dots & 0 \\ 0 & 0 & 1 & 0 & \frac{1}{v_x T_s} & -\frac{1}{v_x T_s} & 0 & \dots & 0 \end{bmatrix} \quad (20)$$

T_s is the sampling interval. The weight matrix $\boldsymbol{C}$ defines the link between the vehicle and road preview. The first row of $\boldsymbol{C}$ is formulated to minimize the sum of the squares of the lateral displacement error, Δy_{CG}, and the second row to minimize the square of the heading error at the center of gravity, calculated as $(\psi_{CG} - \frac{\Delta y_1 - \Delta y_{CG}}{v_x T_s})^2$. After a re-arrangement in local vehicle coordinates (see [37]), the control law is given in eq. (21), with the preview and state feedback gains scheduled with v_x:

$$\begin{bmatrix} \delta \\ M_{z,FB} \end{bmatrix} = \boldsymbol{K_{prv}}(v_x) \begin{bmatrix} v_y \\ \dot{\psi} \\ \Delta y_{CG} \\ \Delta y_1 \\ \vdots \\ \Delta y_{n_p} \end{bmatrix}$$

$$\boldsymbol{K_{prv}}(v_x) = \begin{bmatrix} k_{\delta,\dot{y}_{CG}} & k_{\delta,\dot{\psi}_{CG}} & k_{\delta,\Delta y_{CG}} & k_{\delta,\Delta y_1} & \dots & k_{\delta,\Delta y_{n_p}} \\ k_{M_z,\dot{y}_{CG}} & k_{M_z,\dot{\psi}_{CG}} & k_{M_z,\Delta y_{CG}} & k_{M_z,\Delta y_1} & \dots & k_{M_z,\Delta y_{n_p}} \end{bmatrix} \quad (21)$$

E. LQR_δ and $P\text{-}LQR_\delta$: Linear Quadratic Regulators for Steering Control

In this study the LQRs of Sections III.C and III.D are also considered in their original formulations, reported in [15] and [37], excluding the direct yaw moment. These, respectively indicated as LQR_δ and $P\text{-}LQR_\delta$, can either operate on their own, or can be part of a multi-layer structure, including the TVC presented in Section IV.

IV. Torque-Vectoring Controller (TVC)

A separate TVC was developed to assess the effectiveness of the multi-layer PTC+TVC structures. The details of the TVC design and functionality are presented in [24]. The TVC includes a reference yaw rate generator and a reference yaw moment generator, and together with the PTCs of Section III uses a wheel torque control allocation algorithm.

A. Reference Yaw Rate Generator

The steady-state value of the TVC reference yaw rate, $\dot{\psi}^{TVC}_{ref,SS}$, is the weighted average of two yaw rate values (see [24], [38] and [39]), $\dot{\psi}^{TVC}_{ref,H}$ and $\dot{\psi}^{TVC}_{ref,S}$:

$$\dot{\psi}^{TVC}_{ref,SS} = \dot{\psi}^{TVC}_{ref,H}\ w_\beta + \dot{\psi}^{TVC}_{ref,S}\ (1 - w_\beta) \quad (22)$$

The handling yaw rate, $\dot{\psi}^{TVC}_{ref,H}$, corresponds to the reference steady-state EV cornering behavior in nominal high tire-road friction conditions. $\dot{\psi}^{TVC}_{ref,H}$ is defined in a look-up table, which is a function of steering angle, vehicle speed and longitudinal acceleration. $\dot{\psi}^{TVC}_{ref,H}$ is designed to shape the vehicle understeer characteristics, which can be rather different from those of the uncontrolled vehicle with identical wheel torques on the left- and right-hand sides [16]. The stability yaw rate, $\dot{\psi}^{TVC}_{ref,S}$, is a conservative yaw rate that is compatible with the actual tire-road friction conditions, i.e., it is based on the measured lateral acceleration (a_y) value.

To determine if the EV operates in different conditions from the nominal ones, the sideslip angle of the rear axle, β_r, is considered [38]:

$$\beta_r = \beta - \frac{br}{v_x} \quad (23)$$

Large values of $|\beta_r|$ indicate saturation of the rear lateral tire forces, which can lead to oversteer and, ultimately, vehicle spinning. The weighting factor w_β determines the significance of the $\dot{\psi}^{TVC}_{ref,H}$ and $\dot{\psi}^{TVC}_{ref,S}$ contributions of $\dot{\psi}^{TVC}_{ref,SS}$. When $|\beta_r|$ is lower than a first threshold ($\beta_{r,th,1}$), $\dot{\psi}^{TVC}_{ref,SS}$ is equal to the handling yaw rate, while when $|\beta_r|$ is higher than a second threshold ($\beta_{r,th,2}$), $\dot{\psi}^{TVC}_{ref,SS}$ is equal to the stability yaw rate, with a smooth transition between the two extreme cases:

$$w_\beta = \begin{cases} 1 & \text{if } |\beta_r| < \beta_{r,th,1} \\ \dfrac{\beta_{r,th,2} - |\beta_r|}{\beta_{r,th,2} - \beta_{r,th,1}} & \text{if } \beta_{r,th,1} \le |\beta_r| \le \beta_{r,th,2} \\ 0 & \text{if } |\beta_r| > \beta_{r,th,2} \end{cases} \quad (24)$$

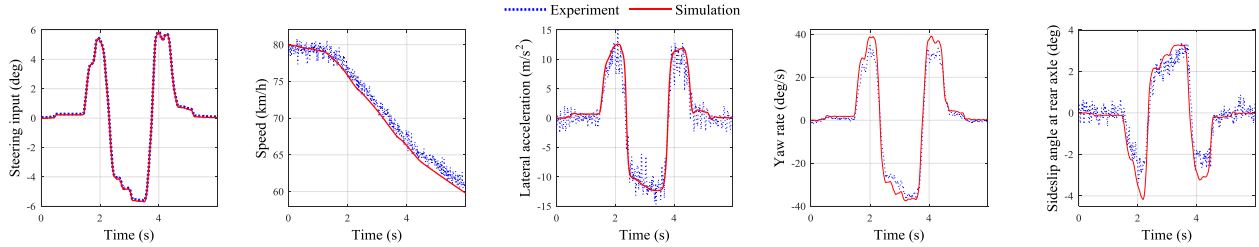

Fig. 4. Experimental validation of the vehicle simulation model in an obstacle avoidance test.

In practice, when the EV operates in low friction or extreme transient conditions, β_r is limited between the two thresholds through the adjustment of $\dot{\psi}^{TVC}_{ref,SS}$. Different sets of thresholds can be defined. In particular, the following two settings are used in this study:

- High sideslip setting: $\beta_{r,th,1} = 4.5$ deg, $\beta_{r,th,2} = 9$ deg, which is adopted in high tire-road friction conditions (tests with $\mu = 1$).
- Low sideslip setting: $\beta_{r,th,1} = 2$ deg, $\beta_{r,th,2} = 4$ deg, which is adopted in low friction conditions (tests with $\mu = 0.6$).

Since the case study EV is for racing applications, the tire-road friction level can be considered approximately known a-priori depending on the condition of the tarmac (e.g., dry or wet), and the switching between the two settings can be imposed without a tire-road friction coefficient estimator. In any case, the simulations and experiments on the case study EV demonstrated that both tunings provide stable and predictable behavior for the whole range of μ values.

A first order transfer function generates the reference yaw rate, $\dot{\psi}^{TVC}_{ref}$, starting from $\dot{\psi}^{TVC}_{ref,SS}$. Note that the resulting $\dot{\psi}^{TVC}_{ref}$, mainly based on δ, differs from the reference yaw rate of the PTCs in Section III, which is purely based on the reference path.

B. Reference Yaw Moment Generator

The reference yaw moment generator is based on a non-linear feedforward contribution and a feedback contribution. The feedforward contribution is computed off-line through a quasi-static model, to achieve $\dot{\psi}^{TVC}_{ref,SS}$ when the EV operates in high tire-road friction conditions with quasi-static steering inputs, and is defined as a look-up table, which is a function of steering angle, vehicle speed and longitudinal acceleration. Similarly to $\dot{\psi}^{TVC}_{ref,SS}$, the feedforward yaw moment contribution is corrected to account for low tire-road friction conditions and transient behavior, based on $|\beta_r|$. The feedback contribution is a proportional integral (PI) controller with anti-windup and gain scheduling with v_x. The reference yaw moment is saturated through the continuous estimation of the EV operational limits, based on the drivetrain torque limits and the estimated individual tire friction limits.

C. Wheel Torque Control Allocator

A wheel torque control allocation scheme determines the individual reference wheel torques. Firstly, the control allocator calculates the total wheel torque required on the left- and right-hand sides of the EV to generate the total reference wheel torque and reference yaw moment. Within each side the torque demand is then distributed proportionally to the estimated vertical tire loads, subject to individual wheel and drivetrain torque limitations. The same wheel torque control allocator is used by the separate TVC and the integrated PTCs, as shown in Fig. 2.

V. Simulation and Control System Optimization Framework

A. Experimentally Validated Simulation Model

A non-linear vehicle dynamics simulation model was implemented in Matlab/Simulink and validated against experimental measurements on the case study EV, with and without the TVC of Section IV. Fig. 4 shows an example of simulation and experimental results for the case study EV during an obstacle avoidance test performed at the Upper Heyford airport, United Kingdom. The good match of the results in a wide range of tests shows that the vehicle model is a reliable tool for control system design and assessment.

B. Obstacle Avoidance

The obstacle avoidance [33] is a vehicle dynamics test to evaluate the transient performance at the cornering limit. Accelerator and brake control is not allowed during the maneuver; therefore it is $T_{w,tot} = 0$. In this study, the lane is 4 m wide and a test is considered successful when all four wheels remain inside the lane boundaries.

For ease of discussion, the obstacle avoidance maneuver is split into five segments. Fig. 5 shows the segments, the lane boundaries, the different reference paths, and the corresponding reference lateral acceleration profile for $v_x = 70$ km/h, calculated as $a_{y,ref} = {v_x}^2 \kappa_{ref}$. The middle line reference path consists of five straight lines, connecting the middle points at each segment transition. This path does not have a continuous curvature profile at the segment transitions, making it unsuitable for the single-point PTCs. Therefore, a standard reference path (RP) with continuous curvature profile is designed by applying a 15 m moving average filter to the middle line path. Additionally, a smooth reference path (smooth RP) is designed by processing the middle line path with a 37.5 m moving average filter. The smooth RP provides a low curvature profile that allows adequate margin with respect to the lane boundaries.

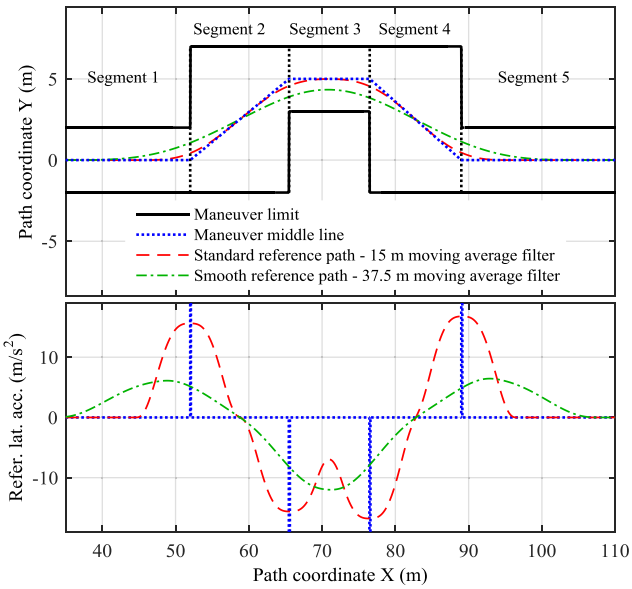

Fig. 5. Reference paths for the obstacle avoidance maneuver ($a_{y,ref}$ calculated for $v_x = 70$ km/h).

C. Tuning Parameters

To ensure a fair comparison, the main tuning parameters of the controllers are optimized to minimize the cost function $J_{Assessment}$, which will be defined in Section V.E.

For the $FF\text{-}FB_\delta$ controller, the optimized parameters are the feedback gain, $K_{FF\text{-}FB_\delta}$, and the look-ahead distance, x_{LA}. For the LQR_{δ,M_z} and $P\text{-}LQR_{\delta,M_z}$, the optimized parameters are the weights associated with the control actions, r_δ and r_{M_z}, the weights associated with the errors, $q_{\Delta y_{CG}}$ and $q_{\Delta\psi_{CG}}$, and the percentage of the maximum lateral acceleration, $p_{a_{y,max}}$, for selecting the cornering stiffness values of the state-space vehicle model. For the LQR_δ and $P\text{-}LQR_\delta$ optimization, the weight associated with the yaw moment control action, r_{M_z}, is set to a high value and omitted from the process. The parameters of the separate TVC are not optimized, as they have been empirically fine-tuned in simulations and experiments on the case study EV.

D. Optimization Method

Evolutionary algorithms are suitable instruments to optimize vehicle handling behavior [40], [41]. A 1 + N evolution strategy (ES) is selected [42], in which a set of N offspring parameter vectors is generated by mutation of a parent vector. The mutation is performed by adding a normally distributed random value to each component of the parent vector. The standard deviation of the normal distribution is the mutation magnitude. An objective function, $J_{Assessment}$, calculated at the end of each obstacle avoidance simulation, determines the fitness of each offspring parameter vector. The parameter vector with the minimum value of $J_{Assessment}$ from the set that includes the offspring vectors and the parent vector is selected as the new parent vector. If the parent vector has remained the same as in the previous generation, the mutation magnitude is decreased, whereas if the parent vector is replaced by an offspring vector, the mutation magnitude is increased to expand the search space. The optimization process terminates when the mutation magnitude decreases below a pre-defined threshold. The PTC parameter optimization was performed for high tire-road friction conditions ($\mu = 1$). In Section VI, the PTCs optimized for $\mu = 1$ will also be assessed by running low friction tests ($\mu = 0.6$) to check the robustness of control system performance.

E. Performance Indicators and Objective Function

The optimization procedure of Section V.D minimizes $J_{Assessment}$, which combines the following performance indicators:

- The entry speed for a successful completion of the test, v_{in}, which must be maximized. As a consequence, within $J_{Assessment}$, v_{in} is multiplied by a relatively large negative weighting factor, $-w_{v_{in}}$, to prioritize high entry speeds.
- The root mean square values of the position error and the heading angle error between the EV trajectory and the reference path during the maneuver:

$$\mathrm{RMS}_{\Delta y_{CG}} = \sqrt{\frac{1}{t_{fin}-t_{in}}\int_{t_{in}}^{t_{fin}} (\Delta y_{CG})^2 dt}$$
$$\mathrm{RMS}_{\Delta\psi_{CG}} = \sqrt{\frac{1}{t_{fin}-t_{in}}\int_{t_{in}}^{t_{fin}} (\Delta\psi_{CG})^2 dt} \quad (25)$$

  where t_{in} and t_{fin} are the initial and final times of the relevant part of the test.
- The integral of the absolute value of the control actions, IACA, which evaluates the steering and yaw moment control efforts:

$$\mathrm{IACA}_\delta = \frac{1}{t_{fin}-t_{in}}\int_{t_{in}}^{t_{fin}} |\delta| dt;$$
$$\mathrm{IACA}_{M_z} = \frac{1}{t_{fin}-t_{in}}\int_{t_{in}}^{t_{fin}} |M_{z,ref}| dt \quad (26)$$

- The difference between the entry speed, v_{in}, and the final speed, v_{fin}. The EV should slow down as little as possible during the maneuver.

The weighting factors w of the performance indicators are selected to normalize the values and define their relative contribution to $J_{Assessment}$, which is given by:

$$\begin{aligned} J_{Assessment} = &-w_{v_{in}} v_{in} + w_{\Delta y_{CG}} \mathrm{RMS}_{\Delta y_{CG}} \\ &+ w_{\Delta\psi_{CG}} \mathrm{RMS}_{\Delta\psi_{CG}} + w_\delta \mathrm{IACA}_\delta \\ &+ w_{M_z} \mathrm{IACA}_{M_z} + w_{v_{fin}} (v_{in} - v_{fin}) \end{aligned} \quad (27)$$

The optimization minimizes $J_{Assessment}$, rather than directly maximizing v_{in}, to ensure a reasonably good quality of the overall EV response during the test. The optimization includes the constraint that the EV must remain within the obstacle avoidance lane boundaries, i.e., the simulations are stopped if this does not happens, and a high value of $J_{Assessment}$ is imposed. The optimization routine changes the values of the elements of the parameter vector, i.e., the tuning parameters of Section V.C,

TABLE II
SUMMARY OF THE MAIN CHARACTERISTICS OF THE ASSESSED PTCS

Controller	Feedback	Feedforward	Preview	Input	Optimized parameters
$FF\text{-}FB_\delta$	P	Yes	No	δ	$K_{FF\text{-}FB_\delta}$, x_{LA}
LQR_{δ,M_z}	LQR	No	No	δ, M_z	r_δ, r_{M_z}, $q_{\Delta y_{CG}}$, $q_{\Delta\psi_{CG}}$, $p_{a_{y,max}}$
$LQR_{\delta,M_z,FF}$	LQR	Yes	No	δ, M_z	
$P\text{-}LQR_{\delta,M_z}$	LQR	No	Yes	δ, M_z	
LQR_δ	LQR	No	No	δ	r_δ, $q_{\Delta y_{CG}}$, $q_{\Delta\psi_{CG}}$, $p_{a_{y,max}}$
$LQR_{\delta,FF}$	LQR	Yes	No	δ	
$P\text{-}LQR_\delta$	LQR	No	Yes	δ	

and calculates $J_{Assessment}$ for increasing values of v_{in}, at increments of 1 km/h, until the EV fails to complete the maneuver.

Section VI also reports additional performance indicators, which are not included in $J_{Assessment}$. They are: i) the maximum absolute value of the rear axle sideslip angle, $|\beta_{r,max}|$, which is an indicator of vehicle stability; and ii) $p_{\delta_{FF}}$ and $p_{M_{z,FF}}$, assessing the significance of the feedfordward contributions in the generation of the reference steering angle and yaw moment:

$$p_{\delta_{FF}} = 100\frac{\text{IACA}_{\delta,FF}}{\text{IACA}_{\delta,FF}+\text{IACA}_{\delta,FB}};$$
$$p_{M_{z,FF}} = 100\frac{\text{IACA}_{M_z,FF}}{\text{IACA}_{M_z,FF}+\text{IACA}_{M_z,FB}} \quad (28)$$

where the subscripts 'FF' and 'FB' refer to the feedforward and feedback contributions, respectively.

VI. RESULTS

The performance of the optimized PTCs is assessed in the obstacle avoidance maneuver simulated with the validated EV model. The results are presented in the following order:

- Section VI.A: The PTCs with preview, i.e., the $P\text{-}LQR_{\delta,M_z}$ and $P\text{-}LQR_\delta$, using the standard reference path (RP).
- Section VI.B: The PTCs without preview, i.e., the $FF\text{-}FB_\delta$, LQR_{δ,M_z}, $LQR_{\delta,M_z,FF}$, LQR_δ and $LQR_{\delta,FF}$, using the standard RP.
- Section VI.C: The PTCs without preview, i.e., the same as in Section VI.B, using the smooth RP.

Table II summarizes the main characteristics of the controllers. Fig. 6 presents a comparison of the trajectories of the EV center of gravity and vehicle envelope for the best performing controller from each group, at $\mu = 1$.

A. PTCs With Preview Using the Standard RP

Table III ranks the PTCs according to the maximum entry speed, $v_{in,max}$, at the completion of the optimization, i.e., once $J_{Assessment}$ is minimized. If $v_{in,max}$ is the same, the PTCs are ranked according to their final $J_{Assessment}$ value. Table III also reports a selection of the individual performance indicators at the respective $v_{in,max}$.

For $\mu = 1$ the integrated steering and yaw moment preview controller, $P\text{-}LQR_{\delta,M_z}$, achieves the highest $v_{in,max}$, i.e., 94 km/h, followed by the $P\text{-}LQR_\delta + TVC$ (92 km/h) and the $P\text{-}LQR_\delta$ (91 km/h). As shown in Fig. 6(a), despite using the standard RP, the $P\text{-}LQR_{\delta,M_z}$ actually follows a path very similar to the smooth RP, and uses most of the available maneuver space, as the EV envelope touches the inner corner limit in all four segment transitions. The deviation from the path is fairly symmetric and the EV converges to the reference path shortly after returning to the original lane.

Fig. 7 reports the obstacle avoidance simulation results at $v_{in} = 94$ km/h. At this speed, the $P\text{-}LQR_\delta + TVC$ and the $P\text{-}LQR_\delta$ fail to pass the test by clipping the lane boundary at the entrance of segment 5, as indicated by the crosses in the lateral position error subplot. The results show a clear improvement of the position error for the integrated controller, $P\text{-}LQR_{\delta,M_z}$, at the transition between segments 4 and 5, when the EV returns to the original lane. The EV with the $P\text{-}LQR_{\delta,M_z}$ experiences high values of $|\dot{\psi}|$ and $|\beta_r|$, which are a symptom of reduced stability, and lower values of steering and yaw moment control actions. The latter can be attributed to the coordinated application of steering and yaw moment control, since the separate TVC of the $P\text{-}LQR_\delta + TVC$, in some cases, applies a yaw moment that opposes the steering action, in order to track $\dot{\psi}_{ref}^{TVC}$.

For $\mu = 0.6$ the situation reverses, since the EV with the $P\text{-}LQR_\delta + TVC$ passes the test at $v_{in} = 71$ km/h, 2 km/h higher than with the $P\text{-}LQR_{\delta,M_z}$. At this entry speed the steering only controller ($P\text{-}LQR_\delta$) fails by briefly going outside the lane at the entrance of segment 5. The $P\text{-}LQR_{\delta,M_z}$ has a lower position error during the transition to segment 5 (similarly to the case of $\mu = 1$), but shortly after, it experiences very high values of $|\dot{\psi}|$ and $|\beta_r|$, and ultimately the vehicle is unstable and spins. On the other hand, the sideslip angle based correction mechanism of the separate $P\text{-}LQR_\delta + TVC$ performs as expected, and ensures stability by adjusting $\dot{\psi}_{ref}^{TVC}$ to limit $|\beta_r|$ between the predefined thresholds. This is an important and novel conclusion of this study. It was also verified that this reliable behavior of the PTCs with separate TVC can be achieved for a very wide range of sideslip thresholds.

B. PTCs Without Preview Using the Standard RP

The performance indicators for the PTCs of this group are reported in Table IV. For $\mu = 1$, the maximum entry speed is 82 km/h, i.e., 12 km/h lower than for the preview PTCs of Section VI.A. The feedforward-feedback steering controller with separate TVC ($FF\text{-}FB_\delta + TVC$) and the integrated steering and yaw moment controllers (LQR_{δ,M_z} and $LQR_{\delta,M_z,FF}$) achieve the same $v_{in,max}$, with the additional performance indicators of $J_{Assessment}$ determining the relative ranking. Fig. 6(b) shows that the EV tracks the path with a significant delay. In contrast to the preview PTCs, the EV is not using the available space at the entrance of segments 2 and 4, as it tries to follow the RP. The EV also shows a slow convergence to the reference path, after entering segment 5.

Fig. 8 compares a selection of controllers at $\mu = 1$ and $v_{in} = 82$ km/h. The steering only controller ($FF\text{-}FB_\delta$) fails the test at the transitions from segment 2 to segment 3 and from segment 4 to segment 5. The steering control input for the compared controllers is similar, while the yaw moment control action of the integrated and separate implementations is significantly different. This is also reflected in the high values of yaw rate and rear axle

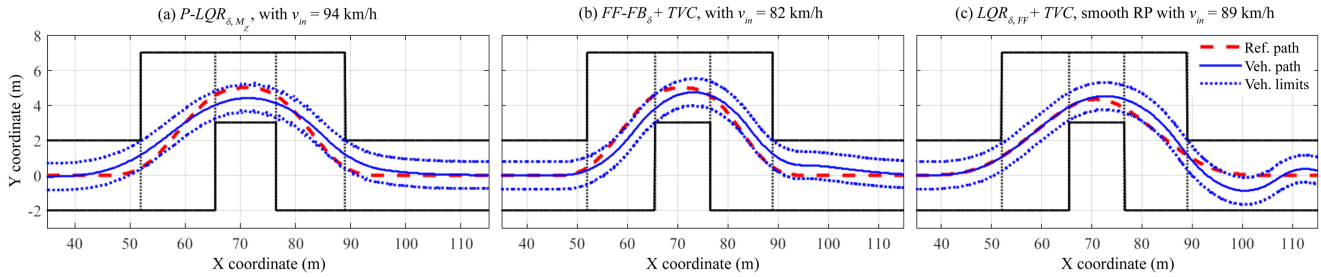

Fig. 6. Comparison of vehicle path and outer limits for the entry speed minimizing $J_{Assessment}$ for each group of controllers. (a) $P\text{-}LQR_{\delta,M_z}$, with $v_{in} =$ 94 km/h. (b) $FF\text{-}FB_{\delta,M_z}$, with $v_{in} = 82$ km/h. (c) $LQR_{\delta,M_z,FF}$, smooth RP with $v_{in} = 89$ km/h.

TABLE III
PERFORMANCE INDICATORS OF THE PTCs WITH PREVIEW USING THE STANDARD RP

Controller	$v_{in,max}$ (km/h)	v_{fin} (km/h)	RMS$_{\Delta y_{CG}}$ (m)	IACA$_\delta$ (deg)	IACA$_{M_z}$ (Nm)	$p_{M_{z,FF}}$ (%)	$\lvert\beta_{r,\max}\rvert$ (deg)
High friction ($\mu = 1$)							
$P\text{-}LQR_{\delta,M_z}$	94	68.95	0.295	1.47	170	-	6.86
$P\text{-}LQR_\delta + TVC$	92	68.11	0.295	1.52	447	75.1%	3.63
$P\text{-}LQR_\delta$	91	67.42	0.304	1.52	-	-	3.48
Low friction ($\mu = 0.6$)							
$P\text{-}LQR_\delta + TVC$	71	48.96	0.270	1.33	303	70.5%	3.37
$P\text{-}LQR_\delta$	70	48.27	0.279	1.47	-	-	2.29
$P\text{-}LQR_{\delta,M_z}$	69	46.42	0.255	1.12	129	-	9.19

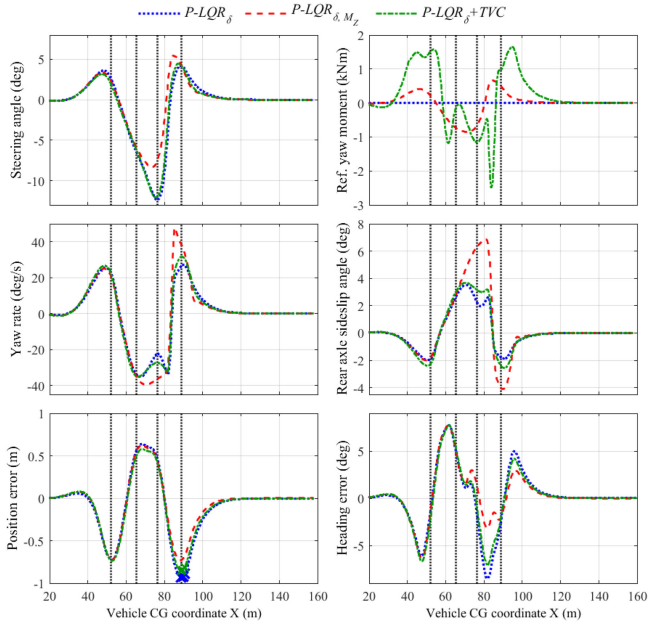

Fig. 7. Obstacle avoidance performed by the preview PTCs using the standard RP at $v_{in} = 94$ km/h and $\mu = 1$ (the dotted vertical lines indicate the segment transitions).

sideslip angle of the integrated steering and yaw moment controller ($LQR_{\delta,M_z,FF}$), which is a consistent characteristic of all the integrated controllers when operating at the limit of handling.

For $\mu = 0.6$, the maximum entry speed of 64 km/h is achieved by the LQR controllers actuating only the steering system, in cooperation with the TVC ($LQR_{\delta,FF} + TVC$ and $LQR_\delta + TVC$). For example, at $v_{in} = 63$ km/h, the integrated steering

TABLE IV
PERFORMANCE INDICATORS OF THE PTCs WITHOUT PREVIEW USING THE STANDARD RP

Controller	$v_{in,max}$ (km/h)	v_{fin} (km/h)	RMS$_{\Delta y_{CG}}$ (m)	IACA$_\delta$ (deg)	$p_{\delta_{FF}}$ (%)	IACA$_{M_z}$ (Nm)	$p_{M_{z,FF}}$ (%)	$\lvert\beta_{r,max}\rvert$ (deg)
High friction ($\mu = 1$)								
$FF\text{-}FB_\delta + TVC$	82	53.56	0.340	2.86	55.1%	332	54.8%	3.57
$LQR_{\delta,M_z,FF}$	82	53.16	0.341	1.93	62.5%	430	55.3%	6.80
LQR_{δ,M_z}	82	52.28	0.343	2.15	-	286	-	5.05
$LQR_{\delta,FF} + TVC$	81	54.21	0.300	1.66	71.4%	282	59.2%	3.65
$FF\text{-}FB_\delta$	81	52.89	0.335	2.96	53.5%	-	-	2.98
$LQR_\delta + TVC$	81	52.19	0.339	2.18	-	318	48.8%	3.72
$LQR_{\delta,FF}$	80	53.95	0.318	1.80	75.9%	-	-	3.38
LQR_δ	79	51.87	0.302	1.31	-	-	-	3.11
Low friction ($\mu = 0.6$)								
$LQR_{\delta,FF} + TVC$	64	40.91	0.289	1.53	72.6%	269	50.8%	3.92
$LQR_\delta + TVC$	64	39.46	0.331	2.22	-	383	39.7%	4.02
$FF\text{-}FB_\delta + TVC$	63	39.17	0.257	2.33	61.0%	347	42.6%	4.06
$FF\text{-}FB_\delta$	63	39.96	0.302	2.53	57.9%	-	-	2.04
$LQR_{\delta,FF}$	62	40.23	0.264	1.66	77.2%	-	-	2.21
LQR_{δ,M_z}	62	37.58	0.286	2.57	-	287	-	3.35
$LQR_{\delta,M_z,FF}$	62	35.26	0.292	1.55	61.4%	444	39.2%	12.80
LQR_δ	61	39.02	0.280	1.21	-	-	-	2.15

and yaw moment controller ($LQR_{\delta,M_z,FF}$) fails the test by exceeding the maneuver limits at the entrance of segment 5.

C. PTCs Without Preview Using the Smooth RP

The performance indicators for this group of PTCs are reported in Table V. For $\mu = 1$ the $v_{in,max}$ of 89 km/h is achieved by the $LQR_{\delta,FF} + TVC$, which is higher than the 81 km/h of the same PTC using the standard RP, but lower than the 94 km/h of the preview PTCs. Fig. 6(c) shows that the EV with the $LQR_{\delta,FF} + TVC$ can closely track the reference path up to the middle of segment 3, however afterwards it experiences significant deviation. Hence, the EV takes much longer to stabilize and converge to the reference path with respect to the case of preview controllers. While the use of a smooth path improves the performance of the PTCs without preview, the EV without a preview PTC performs considerably worse than the same EV with preview PTCs.

A PTC comparison at $\mu = 1$ is presented in Fig. 9, for $v_{in} =$ 89 km/h. The steering control action of the $LQR_{\delta,FF}$ is significant, as shown by the IACA$_\delta$ in Table V. δ is saturated for considerable amount of time by the physical limits of the steering system of the specific EV. Additionally, $p_{\delta_{FF}}$ is less than 10%, compared to the 70–80% for the same controller along the standard RP. This suggests that the accurate tracking

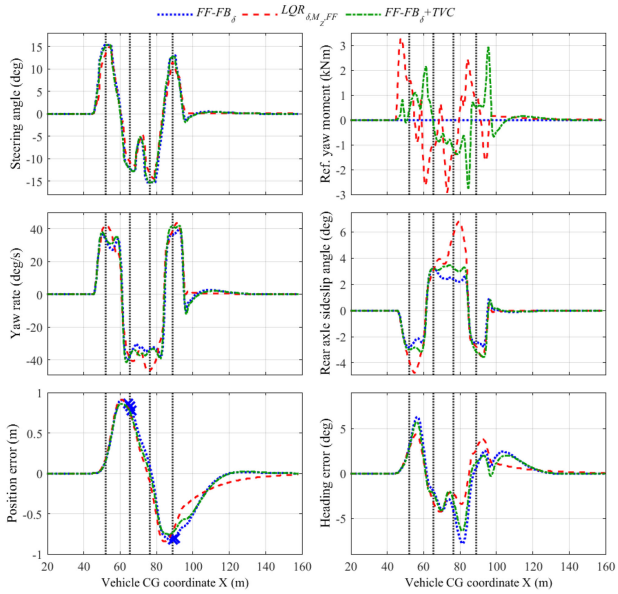

Fig. 8. Obstacle avoidance performed by the PTCs without preview using the standard RP at $v_{in} = 82$ km/h and $\mu = 1$.

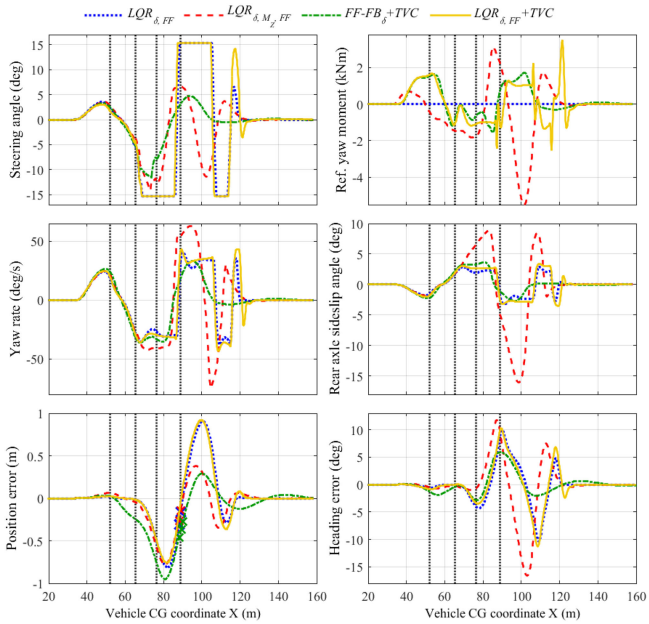

Fig. 9. Obstacle avoidance performed by the PTCs without preview with the smooth RP at $v_{in} = 89$ km/h and $\mu = 1$.

TABLE V
PERFORMANCE INDICATORS OF THE PTCS WITHOUT PREVIEW USING THE SMOOTH RP

Controller	$v_{in,max}$ (km/h)	v_{fin} (km/h)	RMS$_{\Delta y_{CG}}$ (m)	IACA$_\delta$ (deg)	$p_{\delta_{FF}}$ (%)	IACA$_{M_z}$ (Nm)	$p_{M_{z,FF}}$ (%)	$\lvert\beta_{r,\max}\rvert$ (deg)
High friction ($\mu = 1$)								
$LQR_{\delta,FF} + TVC$	89	55.59	0.299	4.97	6.1%	555	53.2%	3.54
$LQR_{\delta,M_z,FF}$	88	60.95	0.179	1.54	44.5%	489	35.9%	7.90
LQR_{δ,M_z}	88	58.53	0.211	3.11	-	274	-	5.08
$LQR_\delta + TVC$	88	58.16	0.227	3.45	-	456	54.0%	3.45
$LQR_{\delta,FF}$	88	56.78	0.246	4.17	9.6%	-	-	3.21
LQR_δ	87	57.06	0.226	3.56	-	-	-	3.20
$FF\text{-}FB_\delta + TVC$	86	62.29	0.185	1.52	57.2%	453	78.3%	3.70
$FF\text{-}FB_\delta$	84	60.76	0.139	1.47	65.5%	-	-	3.15
Low friction ($\mu = 0.6$)								
$LQR_{\delta,FF} + TVC$	71	40.43	0.347	6.08	5.0%	913	35.3%	4.57
$FF\text{-}FB_\delta + TVC$	70	48.31	0.123	1.25	68.4%	308	68.4%	3.70
$LQR_\delta + TVC$	70	42.76	0.251	4.03	-	661	39.2%	4.25
$LQR_{\delta,M_z,FF}$	69	42.87	0.161	1.66	36.4%	741	15.3%	25.71
$LQR_{\delta,FF}$	69	40.84	0.307	5.32	6.6%	-	-	1.99
LQR_{δ,M_z}	68	43.52	0.154	2.60	-	210	-	3.61
LQR_δ	68	41.08	0.268	4.54	-	-	-	1.96
$FF\text{-}FB_\delta$	67	46.11	0.088	1.20	74.0%	-	-	2.28

of the smooth RP requires the use of large feedback gains. During the optimization of the feedforward-feedback controller ($FF\text{-}FB_\delta$), it was observed that the use of higher feedback gains and smaller look-ahead distances increases the v_{in} values for which the EV passes the first four segments of the maneuver. However, during segment 5 this also causes evident oscillations, which are difficult to control because of the use of a proportional gain in the feedback part of the controller. For this reason the optimization ultimately selected lower feedback gains for the $FF\text{-}FB_\delta$, which result in lower steering action but also lower $v_{in,max}$.

For $\mu = 0.6$ the $LQR_{\delta,FF} + TVC$ achieves the top $v_{in,max} = 71$ km/h, followed by the $FF\text{-}FB_\delta + TVC$ and the $LQR_\delta + TVC$, with $v_{in,max} = 70$ km/h. However, as shown by the performance indicators in Table V, these results are obtained through very different actuation profiles. In fact, the $LQR_{\delta,FF} + TVC$ has a IACA$_\delta = 6.08$ deg, and a IACA$_{M_z} = 913$ Nm, i.e., this tuning of the PTC is characterized by over-actuation of the steering system and yaw moment. The $FF\text{-}FB_\delta + TVC$ has a IACA$_\delta = 1.25$ deg, and a IACA$_{M_z} = 308$ Nm, with reduced lateral tire slip power losses, which result in a large difference in v_{fin}, i.e., of almost 8 km/h in favor of the $FF\text{-}FB_\delta + TVC$. The integrated steering and yaw moment controller, $LQR_{\delta,M_z,FF}$, similarly to all previous cases, experiences very high values of $|\dot{\psi}|$ and $|\beta_r|$.

VII. CONCLUSIONS

This study compared the performance of different path tracking controllers with integrated or separate torque-vectoring functionality during obstacle avoidance tests. The assessment was based on an experimentally validated electric vehicle simulation model. To ensure an objective comparison, the control system parameters were fine-tuned through a genetic algorithm, which was run for high tire-road friction conditions, while the control system assessment covered low friction conditions as well. Two reference paths, i.e., a standard reference path and a smooth reference path, were given as inputs to the controllers. The main conclusions are:

- The path tracking controllers with road preview information and the standard reference path achieve the highest entry speed.
- The use of a smooth reference path, similar to the path followed by the preview controllers, increases the maximum entry speed achievable with the controllers without preview, at the expense of increased oscillations after the vehicle returns to the original lane.

- Continuously active torque-vectoring control, either with integrated or separate multi-layer implementations, improves vehicle performance compared to path tracking control only based on the steering system actuation. More specifically, torque-vectoring increases $v_{in,max}$ by 1 to 3 km/h with respect to the EV with the same PTC, but excluding direct yaw moment control.
- In the formulations without preview, the use of a feedforward contribution for steering and yaw moment actuation is usually beneficial to both the integrated and separate controllers, with an increase of $v_{in,max}$ of up to 2 km/h.
- The integrated steering and yaw moment controllers can achieve high entry speeds, and thus enhanced vehicle agility, especially if they include a preview component in their formulation, and are tuned for the specific tire-road friction condition. Therefore, the integrated control structures can be recommended for race vehicle applications, such as the EV of this study, which operates on race tracks, with at least approximately known friction conditions. However, the integrated solutions tend to give origin to very variable behavior when they operate at different friction coefficients. In particular, the integrated controllers provoked very high values of $|\beta_r|$ in many of the tests at $\mu = 0.6$, because of the intrinsic lack of consideration of vehicle stability and cornering limits in their formulations.
- The separate TVC guarantees consistently safe and stable EV response, with $|\beta_r|$ saturation according to the specified thresholds. Based on these results, the multi-layer control structures are recommended for future passenger car implementations. As a consequence, the wide literature already available on the topic of torque-vectoring control of human-driven EVs with multiple motors remains meaningful and valid also for the design of TVCs for autonomous EVs.

The next steps of this research will be focused on the experimental validation of these simulation results and the analysis of the effect of parameter uncertainties and disturbances.

REFERENCES

[1] A. Sorniotti, P. Barber, and S. De Pinto, "Path tracking for automated driving: A tutorial on control system formulations and ongoing research," in *Automated Driving: Safer and More Efficient Future Driving*, D. Watzenig and M. Horn, Eds. New York, NY, USA: Springer, 2017, pp. 71–140.

[2] C. Chatzikomis and K. N. Spentzas, "A path-following driver model with longitudinal and lateral control of vehicle's motion," *Eng. Res.*, vol. 73, no. 4, pp. 257–266, 2009.

[3] J. Edelmann, M. Plöchl, W. Reinalter, and W. Tieber, "A passenger car driver model for higher lateral accelerations," *Veh. Syst. Dyn.*, vol. 45, no. 12, pp. 1117–1129, 2007.

[4] C. C. MacAdam, "Application of an optimal preview control for simulation of closed-loop automobile driving," *IEEE Trans. Syst. Man. Cybern.*, vol. SMC-11, no. 6, pp. 393–399, Jun. 1981.

[5] G. Markkula, O. Benderius, K. Wolff, and M. Wahde, "A review of near-collision driver behavior models," *Hum. Factors*, vol. 54, no. 6, pp. 1117–1143, 2012.

[6] M. Plöchl and J. Edelmann, "Driver models in automobile dynamics application," *Veh. Syst. Dyn.*, vol. 45, nos. 7–8, pp. 699–741, 2007.

[7] R. S. Sharp, D. Casanova, and P. Symonds, "A mathematical model for driver steering control, with design, tuning and performance results," *Veh. Syst. Dyn.*, vol. 33, pp. 289–326, 2000.

[8] R. Attia, R. Orjuela, and M. Basset, "Combined longitudinal and lateral control for automated vehicle guidance," *Veh. Syst. Dyn.*, vol. 52, no. 2, pp. 261–279, 2014.

[9] A. Carvalho, S. Lefévre, G. Schildbach, J. Kong, and F. Borrelli, "Automated driving: The role of forecasts and uncertainty—A control perspective," *Eur. J. Control*, vol. 24, pp. 14–32, 2015.

[10] P. Falcone, F. Borrelli, J. Asgari, H. E. Tseng, and D. Hrovat, "Predictive active steering control for autonomous vehicle systems," *IEEE Trans. Control Syst. Technol.*, vol. 15, no. 3, pp. 566–580, May 2007.

[11] K. Kritayakirana and J. C. Gerdes, "Using the centre of percussion to design a steering controller for an autonomous race car," *Veh. Syst. Dyn.*, vol. 50, no. 1, pp. 33–51, 2012.

[12] G. Tagne, R. Talj, and A. Charara, "Higher-order sliding mode control for lateral dynamics of autonomous vehicles, with experimental validation," in *Proc. IEEE Intell. Veh. Symp.*, 2013, pp. 678–683.

[13] S. Thrun *et al.*, "Stanley: The robot that won the DARPA grand challenge," *Springer Tracts Adv. Robot.*, vol. 36, pp. 1–43, 2007.

[14] F. Roselli *et al.*, "H-infinity control with look-ahead for lane keeping in autonomous vehicles," in *Proc. IEEE Conf. Control Technol. Appl.*, 2017, pp. 2220–2225.

[15] J. M. Snider, "Automatic steering methods for autonomous automobile path tracking," Carnegie Mellon Univ., Pittsburgh, PA, USA, Report CMU-RI-TR-09-08, 2009.

[16] L. De Novellis *et al.*, "Direct yaw moment control actuated through electric drivetrains and friction brakes: Theoretical design and experimental assessment," *Mechatronics*, vol. 26, pp. 1–15, 2015.

[17] Q. Lu *et al.*, "Enhancing vehicle cornering limit through sideslip and yaw rate control," *Mech. Syst. Signal Process.*, vol. 75, pp. 455–472, 2016.

[18] M. Canale, L. Fagiano, A. Ferrara, and C. Vecchio, "Comparing internal model control and sliding mode approaches for vehicle yaw control," *IEEE Trans. Intell. Transp. Syst.*, vol. 10, no. 1, pp. 31–41, Mar. 2009.

[19] T. Goggia *et al.*, "Integral sliding mode for the torque-vectoring control of fully electric vehicles: Theoretical design and experimental assessment," *IEEE Trans. Veh. Technol.*, vol. 64, no. 5, pp. 1701–1715, May 2015.

[20] J. S. Hu, Y. Wang, H. Fujimoto, and Y. Hori, "Robust yaw stability control for in-wheel motor electric vehicles," *IEEE/ASME Trans. Mechatron.*, vol. 22, no. 3, pp. 1360–1370, Jun. 2017.

[21] H. Fujimoto and K. Maeda, "Optimal yaw-rate control for electric vehicles with active front-rear steering and four-wheel driving-braking force distribution," in *Proc. 39th Annu. Conf. IEEE Ind. Electron. Soc.*, 2013, pp. 6514–6519.

[22] M. Corno, M. Tanelli, I. Boniolo, and S. M. Savaresi, "Advanced yaw control of four-wheeled vehicles via rear active differential steering," in *Proc. 48th IEEE Conf. Decis. Control 28th Chin. Control Conf.*, 2009, pp. 5176–5181.

[23] R. de Castro, M. Tanelli, R. E. Araújo, and S. M. Savaresi, "Minimum-time manoeuvring in electric vehicles with four wheel-individual-motors," *Veh. Syst. Dyn.*, vol. 52, no. 6, pp. 824–846, 2014.

[24] C. Chatzikomis, A. Sorniotti, P. Gruber, M. Bastin, R. M. Shah, and Y. Orlov, "Torque-vectoring control for an autonomous and driverless electric racing vehicle with multiple motors," *SAE Int. J. Veh. Dyn., Stability, NVH*, vol. 1, no. 2, pp. 338–351, 2017.

[25] S. T. Peng, C. C. Hsu, and C. C. Chang, "On a robust bounded control design of the combined wheel slip for an autonomous 4WS4WD ground vehicle," *Veh. Syst. Dyn.*, vol. 2005, no. 5, pp. 6504–6509, 2005.

[26] H. Okajima, S. Yonaha, N. Matsunaga, and S. Kawaji, "Direct yaw-moment control method for electric vehicles to follow the desired path by driver," in *Proc. SICE Annu. Conf.*, 2010, pp. 642–647.

[27] R. Wang, C. Hu, F. Yan, and M. Chadli, "Composite nonlinear feedback control for path following of four-wheel independently actuated autonomous ground vehicles," *IEEE Trans. Intell. Transp. Syst.*, vol. 17, no. 7, pp. 2063–2074, Mar. 2016.

[28] B. Li, H. Du, and W. Li, "A potential field approach-based trajectory control for autonomous electric vehicles with in-wheel motors," *IEEE Trans. Intell. Transp. Syst.*, vol. 18, no. 8, pp. 2044–2055, Aug. 2017.

[29] C. Hu, R. Wang, F. Yan, and N. Chen, "Output constraint control on path following of four-wheel independently actuated autonomous ground vehicles," *IEEE Trans. Veh. Technol.*, vol. 65, no. 6, pp. 4033–4043, 2016.

[30] A. Goodarzi, A. Sabooteh, and E. Esmailzadeh, "Automatic path control based on integrated steering and external yaw-moment control," *Proc. Inst. Mech. Eng. K, J. Multi-body Dyn.*, vol. 222, no. 2, pp. 189–200, 2008.

[31] P. Falcone, H. Eric Tseng, F. Borrelli, J. Asgari, and D. Hrovat, "MPC-based yaw and lateral stabilisation via active front steering and braking," *Veh. Syst. Dyn.*, vol. 46, no. 1, pp. 611–628, 2008.

[32] F. Yakub and Y. Mori, "Comparative study of autonomous path-following vehicle control via model predictive control and linear quadratic control," *Proc. Inst. Mech. Eng. D, J. Automobile Eng.*, vol. 229, no. 12, pp. 1695–1714, 2015.
[33] *Passenger Cars — Test Track for a Severe Lane-Change Manoeuvre Part 2: Obstacle Avoidance*, ISO Standard 3888-2:2011, 2011.
[34] N. R. Kapania and J. C. Gerdes, "Design of a feedback-feedforward steering controller for accurate path tracking and stability at the limits of handling," *Veh. Syst. Dyn.*, vol. 53, no. 12, pp. 1687–1704, 2015.
[35] Q. Lu, A. Sorniotti, P. Gruber, J. Theunissen, and J. De Smet, "H∞ loop shaping for the torque-vectoring control of electric vehicles: Theoretical design and experimental assessment," *Mechatronics*, vol. 35, pp. 32–43, 2016.
[36] E. Ostertag, *Mono- and Multivariable Control and Estimation*. New York, NY, USA: Springer, 2011.
[37] R. S. Sharp and V. Valtetsiotis, "Optimal preview car steering control," in *Proc. Sel. Pap. 20th Int. Congr. Theor. Appl. Mech.*, 2001, pp. 101–117.
[38] B. Lenzo, A. Sorniotti, P. Gruber, and K. Sannen, "On the experimental analysis of single input single output control of yaw rate and sideslip angle," *Int. J. Autom. Technol.*, vol. 18, no. 5, pp. 799–811, 2017.
[39] M. Jalali, E. Ashemi, A. Khajepour, S. Chen, and B. Litkouhi, "Integrated model predictive control and velocity estimation of electric vehicles," *Mechatronics*, vol. 46, pp. 84–100, 2017.
[40] M. Gobbi, I. Haque, P. Y. Papalambros, and G. Mastinu, "Optimization and integration of ground vehicle systems," *Veh. Syst. Dyn.*, vol. 43, nos. 6–7, pp. 437–453, 2005.
[41] H. Haghiac, I. Haque, and G. Fadel, "An assessment of a genetic algorithm-based approach for optimising multi-body systems with applications to vehicle handling performance," *Int. J. Veh. Des.*, vol. 36, no. 4, pp. 320–344, 2004.
[42] H. G. Beyer, *The Theory of Evolution Strategies*. New York, NY, USA: Springer, 2013.

Christoforos Chatzikomis received the M.Sc. and Ph.D. degrees in mechanical engineering from the National Technical University of Athens, Athens, Greece, in 2003 and 2010, respectively. Between 2015 and 2017, he was a Research Fellow in electric vehicle control with the University of Surrey, Guildford, U.K. Since 2018, he has been working as a Control Systems Engineer with Roborace, Oxford, U.K. His main research interests include vehicle dynamics, electric vehicle control, and autonomous vehicles.

Aldo Sorniotti (M'12) received the M.Sc. degree in mechanical engineering and the Ph.D. degree in applied mechanics from the Politecnico di Torino, Turin, Italy, in 2001 and 2005, respectively. He is a Professor in advanced vehicle engineering with the University of Surrey, Guildford, U.K., where he coordinates the Centre for Automotive Engineering. His research interests include vehicle dynamics control and transmission systems for electric and hybrid vehicles.

Patrick Gruber received the M.Sc. degree in motorsport engineering and management from Cranfield University, Cranfield, U.K., in 2005, and the Ph.D. degree in mechanical engineering from the University of Surrey, Guildford, U.K., in 2009. He is a Senior Lecturer in advanced vehicle systems engineering with the University of Surrey. His current research interests include vehicle and tire dynamics, and the development of novel tire and rubber friction models.

Mattia Zanchetta received the B.Sc. degree in electronic engineering and telecommunications and the M.Sc. degree in control engineering from the University of Pavia, Pavia, Italy, in 2013 and 2016, respectively. He is currently a Ph.D. Researcher at the University of Surrey, Guildford, U.K. His current research interests include vehicle dynamics control, vehicle testing, and autonomous driving.

Dan Willans received the M.Eng. degree in mechanical engineering from the University of Surrey, Guildford, U.K., in 2016. Since July 2016, he has been working as a Control Systems Engineer with Roborace, Oxford, U.K. His main activities include delivering software and hardware solutions for the vehicles developed by Roborace.

Bryn Balcombe received a degree in mechanical engineering and vehicle design from the University of Hertfordshire, Hatfield, U.K., in 1996. He is the Chief Technology Officer with Roborace, Oxford, U.K, the world's first driverless electric racing series. His experience spans 16 years working with Bernie Ecclestone's Formula One Management leading all significant technical projects from the construction of new circuits to fully automated cars and camera tracking systems, and the implementation of the Formula One Global Media Network. He left to join the executive team of a media start up pioneering multiple cutting edge technologies for TV studios and has also consulted on technology strategy for organisations including the BBC and McCann Worldgroup.